frontiers in Physics

ORIGINAL RESEARCH
published: 09 April 2020
doi: 10.3389/fphy.2020.00078

$LiInSe_2$ for Semiconductor Neutron Detectors

Alireza Kargar, Huicong Hong, Joshua Tower, Andrey Gueorguiev, Hadong Kim, Leonard Cirignano, James F. Christian, Michael R. Squillante and Kanai Shah*

Radiation Devices Inc. (RMD), Watertown, MA, United States

Lithium indium selenide ($LiInSe_2$) is being developed for use as a room temperature semiconductor detector for thermal neutrons. The material has been studied for a number of applications including non-linear optics such as parametric oscillators, as anode material for lithium ion batteries, piezoelectrics, as a scintillation detector material, and as a semiconductor detector material. The recent advances of the crystal growth, material processing, and detector fabrication have led to semiconductor neutron detectors with up to 100 mm^2 active area. The theoretical thermal neutron detection sensitivity and gamma rejection ratio (GRR) are comparable to 10 atm, ^{3}He tubes of similar size. Detector fabrication and characterization are described and the results are discussed.

Keywords: enriched Li, ^{6}Li, thermal neutron detection, detector, $LiInSe_2$, semiconductor and lithium indium selenide

OPEN ACCESS

Edited by:
Paul Sellin,
University of Surrey, United Kingdom

Reviewed by:
Amir Bahadori,
Kansas State University, United States
Bin-Bin Zhang,
Northwestern Polytechnical University, China

****Correspondence:***
Alireza Kargar
akargar@rmdinc.com

Specialty section:
This article was submitted to Radiation Detectors and Imaging, a section of the journal Frontiers in Physics

Received: *28 October 2019*
Accepted: *05 March 2020*
Published: *09 April 2020*

Citation:
Kargar A, Hong H, Tower J, Gueorguiev A, Kim H, Cirignano L, Christian JF, Squillante MR and Shah K (2020) $LiInSe_2$ for Semiconductor Neutron Detectors. Front. Phys. 8:78. doi: 10.3389/fphy.2020.00078

INTRODUCTION

Semiconductors with one or more constituent neutron sensitive isotopes have potential for compact, efficient thermal neutron detection [1]. **Table 1** shows neutron sensitive isotopes with relatively high thermal neutron interaction cross sections along with reaction products and energies. Reactions that yield charged particles with ranges much shorter than the semiconductor dimensions are desired for neutron detection. Unlike conversion layered devices, the detection efficiency of semiconductor devices that incorporate thermal neutron sensitive isotopes as a constituent would not be limited by the short range of charged particle reaction products in the converter layer. In this paper, we report on $LiInSe_2$ semiconductors for thermal neutron as well as its capability for pulse height gamma-ray rejection.

$LiInSe_2$ has a wide bandgap and high resistivity, allowing for detectors for room-temperature operation with low noise (low leakage current) [2]. Several crystals of $LiInSe_2$ with varying conditions were grown and characterized. The optical transmission spectroscopy measurement along with resistivity measurement were performed on many $LiInSe_2$ samples and the results are reported for one representative sample. A moderated ^{241}AmBe fast neutron source was used as the source for thermal neutrons to investigate the device neutron response. Further, the gamma-ray response to ^{60}Co source was measured and the results of the neutron/gamma-ray response are reported.

CALCULATED ABSORPTION

The reactions used in traditional neutron detectors are listed in **Table 1**. Considering the *Q*-value listed in **Table 1**, the $^6Li(n,\alpha)^3H$ reaction gives off charged particles with higher energy, resulting in better neutron-gamma ray discrimination. ^{6}Li has the highest thermal neutron absorption

TABLE 1 | The thermal neutron reaction and the corresponding *Q*-values and absorption cross sections.

Reaction	*Q*-value (MeV)	Cross section, σ (barns)
$^3He+n \rightarrow {}^3H+p$	0.764	5330
$^6Li+n \rightarrow {}^3H+\alpha$	4.780	940
$^{10}B+n \rightarrow {}^7Li+\alpha$	2.310 (94%) 2.792 (6%)	3840

cross section (940 barns) in ^{6}LiInSe$_2$ composition, which makes the macroscopic thermal neutron absorption cross section of ^{6}LiInSe$_2$ composition relatively high. This cross section can be evaluated from the basic relations (labeled as Equation 1) as:

$$\Sigma = \frac{\rho \, \mathbf{N_a} \, \sigma_{\mathbf{tot}}}{\mathbf{A}} \tag{1}$$

where for a given material composition, Σ is the macroscopic thermal neutron absorption cross section of the composition in cm^{-1}, σ_{tot} is the summation of microscopic thermal neutron absorption cross sections of all elements in the composition in barns ($\sigma_{tot} = \sigma_{Li} + \sigma_{In} + 2\sigma_{Se}$), ρ is the density of the composition in grams per cm^3, N_a is the Avogadro's number and A is the molecular weight of the composition in grams per mole. If 100% of lithium atoms are ^{6}Li in ^{6}LiInSe$_2$ compound, Σ can be evaluated as 11.2 cm^{-1} [3, 4], given density of 4.47 g cm^{-3} for the compound and the microscopic thermal neutron absorption cross section of the elements, σ, as: 940 barns for ^{6}Li atoms, 193.8 barns for indium atoms and 11.7 barns for Se atoms. Note that, only the $^6Li(n,\alpha)^3H$ reaction gives off charged particles for the detection application and has the highest absorption cross section among all elements of the composition. The thermal neutrons that interact with In and Se atoms are absorbed in the composition but are not detected. Based on the 11.2 cm^{-1} absorption cross section, a 2.0 mm thick ^{6}LiInSe$_2$ crystal absorbs 89% of the thermal neutrons (intrinsic absorption efficiency) based on the following relation (labeled as Equation 2), where t is the thickness of the crystal in cm:

$$\text{Intrinsic absoption efficiency} = 1 - e^{-\Sigma \, t} \tag{2}$$

The contribution from ^{6}Li to the absorbed thermal neutrons is: $\frac{\sigma_{6Li}}{\sigma_{tot}}$ (= 0.82). In other words 82% of the total absorbed thermal neutrons will experience the $^6Li(n,\alpha)^3H$ reaction, and can be detected. In comparison, a 2.0 mm thickness of ^{3}He at 10 atm absorbs only 32% of thermal neutrons, which is based on macroscopic thermal neutron absorption cross section of 1.9 cm^{-1} for ^{3}He at 10 atm based on Equation (1) or Scattering Length Density Calculator [3].

EXPERIMENTAL PROCEDURE

Crystal Growth

^{6}LiInSe$_2$ crystals were grown by the Vertical Bridgman (VB) technique, following methods described in the literature [2, 5–7]. Semiconductor grade high-purity indium and selenium were purchased from Sigma-Aldrich. Enriched ^{6}Li was obtained from the Y-12 Isotope office at Oak Ridge National Laboratory in Oak Ridge Tennessee. The LiInSe$_2$ was synthesized in two steps: first by reaction of lithium metal with indium metal in the melt at 1,000°C contained in a pBN crucible, which is sealed under vacuum in a larger quartz ampoule along with selenium beads at the bottom of the ampoule. Selenium vapor reacts with lithium-indium molten alloy to form LiInSe$_2$. LiInSe$_2$ crystals are then grown in the same pBN crucible using the vertical Bridgman crystal growth method in a 2-zone Mellon furnace. **Figure 1** shows an ingot removed from the growth ampoule. As can be seen in the figure, the crystal has a chartreuse-yellow color. Note that the voids, on the surface of the ingot, are due to bubbles that form on the surface during the melting of the Li and In metals.

FIGURE 1 | ^{6}LiInSe$_2$ ingot (G77) after crystal growth.

FIGURE 2 | The fabricated planar detector from ingot G77 (labeled as ^{6}LiInSe$_2$-G77-6) with 0.7 mm thickness and 8 mm Fe contact diameter. The sample is wired using 2 mil Pd wire attached to Fe contacts on both side with carbon paste. The planar detector is mounted on a 1 square inch ceramic substrate using RTV Si based glue.

Detector Fabrication

Once the LiInSe$_2$ crystals were taken out of the ampoule, they were cut, and polished. The polished crystals had average final thickness of 0.7 mm. The samples were cleaned with cyclohexane prior to contact deposition. Optical transmission measurements were performed at this stage on the samples, as will be discussed later. Iron was deposited as the metal contacts (typical thickness of 500 angstroms and 8 mm in diameter) on both sides of each

TABLE 2 | Characteristics of LiInSe$_2$ crystals and devices.

Growth #	Enriched Li-6	Optical transmission data		Name of detector(s) tested	Contacts material	Resistivity (Ω cmm)	Ohmic behavior	Neutron response (AmBe)	Gamma ray response
		Samples) prepared	Wavelength (nm) bandgap (eV)						
G50	No			G50-1	CrAu			Yes	Yes (Co-60)
				G50-4	Pt	1.6×10^{11}	yes		
				G50-6-2	Polymer	1.2×10^{12}	yes		Yes (Co-60)
				G50-6-3-1	CrAu	2.1×10^{11}	yes		Yes (Co-60)
				G50-6-3-2	Polymer	6.2×10^{11}	Yes	Yes	Yes (Co-60)
G52	No			G52-7-3	CrAu	3.8×10^{11}	Yes		
				G52-7-4	CrAu	3.3×10^{11}	yes		
G54	Yes	G54-1,2,5,7	436-438nm/2.83-2.84 eV	G54-7	CrAu Pt	1.2×10^{11}	Yes	Yes	Yes (Cs-137)
				G54-5	Pt	1.2×10^{12}	Yes		
				G54-6-1	Polymer	5.2×10^{12}	Yes		Yes (Co-60)
				G54-6-2	Polymer	5.6×10^{12}	Yes	Yes	
				G54-6-3-2	Polymer			Yes	Yes (Co-60)
				G54-5-Fe-Polymer	Fe / Polymer	$1.5\text{-}1.7 \times 10^{11}$	Yes		Yes (Co-60)
G55	No	G55-1,3,5	434-436nm/2.84–2.86 eV						
G58	No			G58-4	CrAu	2.6×10^{11}	Yes		
				G58-6	CrAu	8.7×10^{11}	Yes		
G65	Yes			G65-3	Polymer	$6.2\text{-}7.8 \times 10^{11}$	Yes	yes	Yes (Co-60)
				G65-2	Fe / Polymer	$4.3\text{-}6.7 \times 10^{11}$	Yes		Yes (Co-60)
G66	Yes	G66-2 Tail/Middle/con	440 nm/2.82 eV e						
G67	Yes	G67-1,2	438 nm/2.83 eV						
G68	Yes			G68-1	Fe / Au	1.6×10^{11}	Yes		
				G68-2	Fe / Au	2.1×10^{11}	Yes		
				G68-4	Fe / Au	1.4×10^{11}	Yes		
				G68-Tip	Fe / Au			yes	Yes (Co-60)
				G68-T1	Fe	1.7×10^{11}			No (Co-60)
				G68-T4	Fe	1.5×10^{10}	Yes		
G70	Yes			G70-8	Fe	7.0×10^{10}	Yes		
				G70-9	Fe	1.8×10^{11}			
				G70-10	Fe	$0.1 \times 10^{11}\text{-}7.4 \times 10^{1}$	Yes		
				G70-11	Fe	4.6×10^{11}			
				G70-14	Fe	$0.2 \times 10^{11}\text{-}1.2 \times 10^{1}$	Yes	Yes	
				G70-15	Fe	$0.0 \times 10^{11}\text{-}2.1 \times 10^{1}$	Yes	Yes	Yes (Co-60)
				G70-16	Fe	3.3×10^{11}	YES		Yes (Co-60)
				G70-17	Fe	$0.5 \times 10^{11}\text{-}1.7 \times 10^{1}$			
				G70-18	Fe	$0.3 \times 10^{11}\text{-}1.8 \times 10^{1}$	Yes		
				G70-12	Fe	7.9×10^{11}			
G77	Yes	G77-2,4,11	434 nm/2.86 eV	G77-4	Fe	4.7×10^{11}	Yes	yes	Yes (Co-60)
				G77-5-1	Fe	3.9×10^{11}	Yes	yes	Yes (Co-60)
				G77-5-2	Fe	3.9×10^{11}	Yes	yes	Yes (Co-60)
				G77-6	Fe	3.0×10^{11}	Yes	yes	Yes (Co-60)
				G77-7	Fe	4.5×10^{11}	Yes	No	No

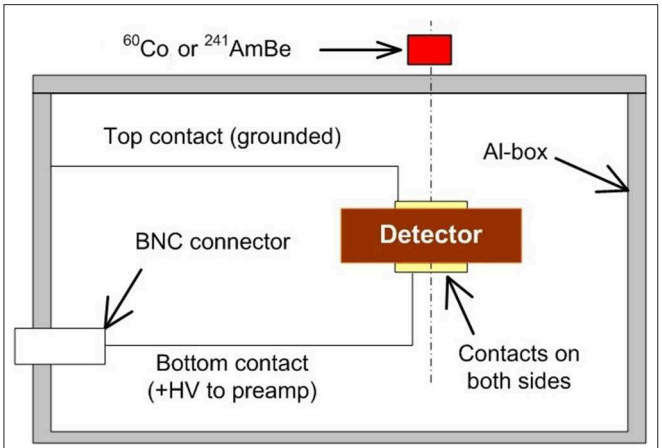

FIGURE 3 | Schematic of test setup with ^{241}AmBe neutron source and ^{60}Co gamma-ray source.

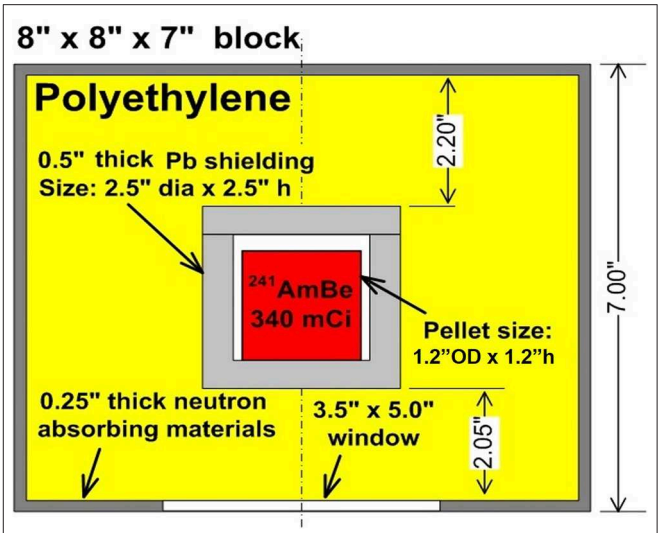

FIGURE 4 | The RMD custom designed casing for the ^{241}AmBe neutron source. The source holder geometry is designed in a way that most of the fast neutrons are thermalized by the polyethylene (as moderator) before reaching the detector. The "dia." on the figure is the acronym for diameter.

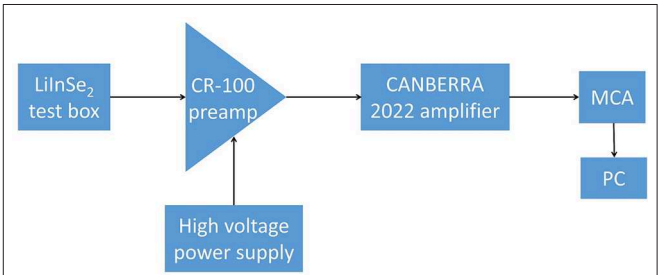

FIGURE 5 | Schematic of the detector test circuit.

sample through thermal evaporation. Carbon paste was used to attach 0.05 mm (2 mil) Pd wires to the Fe contacts. Note that Au, Cr, and Pt have also been previously used and all metals have shown good performances. Fe, however, was the most stable of the metals for the longevity of the LiInSe$_2$ detectors. In other words, the detector was not degraded over time. The samples were then mounted on ceramic substrates using RTV Si based glue for further characterization. **Figure 2** shows the detector, labeled as ^{6}LiInSe$_2$-G77-6, fabricated from ingot G77. Thirty eight samples were fabricate and tested from different ingots; data for one representative ^{6}Li enriched detector is reported in this paper.

Table 2 shows data from 38 devices fabricated from wafers cut from eleven LiInSe$_2$ crystal ingots. The data include the optical transmission spectra, resistivity, and the neutron and gamma-ray response. The bandgap was estimated from the transmission spectra for five samples to be 2.82–2.86 eV. All 38 eight samples were similar in color. Devices were tested with a variety of electrode materials including Cr/Au, Fe, Fe/Au, conducting polymer, and Fe/Polymer. Iron electrodes provided the best stability. Resistivity calculated from IV data ranged from about 1×10^{11} to $6 \times 10^{12}\Omega$-cm Thirty six of the detectors detected both gamma rays and neutrons.

Detector Characterization

Three measurements were employed for characterization of the samples: current-voltage (I-V) measurements, optical transmission measurements, and pulse height spectrum measurements (neutrons and gamma rays). Optical transmission from 400 to 800 nm was conducted at room temperature using a Cary spectrometer. The results of the optical transmission spectroscopy measurements are presented in Results section. A programmable Keithley current-voltage (I-V) characteristic measurement system was used to monitor and record the current at different biases. A linear behavior was observed for both forward and reverse bias, indicating ohmic behavior of Fe/LiInSe$_2$ interface. The values for the resistivity along with the I-V characteristic curve for one of the samples is presented below.

A Tennelec high voltage power supply (HVPS), a CR-110 Cremat preamplifier, a CANBERRA 2022 amplifier and a multi-channel analyzer (MCA) were used to monitor and acquire pulse height. The top contact of the detectors was grounded and the bottom contact was positively biased at +300 V through the preamplifier. The amplifier gain was set to 210×, 8 μs shaping time and positive polarity. The test box with detector, connections, and sources for neutron/gamma-ray counting measurements is shown in **Figure 3**. With the above mentioned setup, pulse height spectra were collected from all samples with a moderated ^{241}AmBe neutron source and ^{60}Co gamma-ray source. Note that the ^{241}AmBe neutron source has a custom designed casing as illustrated in **Figure 4** to facilitate the thermalization of neutrons leaving the bottom of the casing. The schematic of the measurement setup is shown in **Figure 5**. The results of device response to neutrons and gamma rays are reported below.

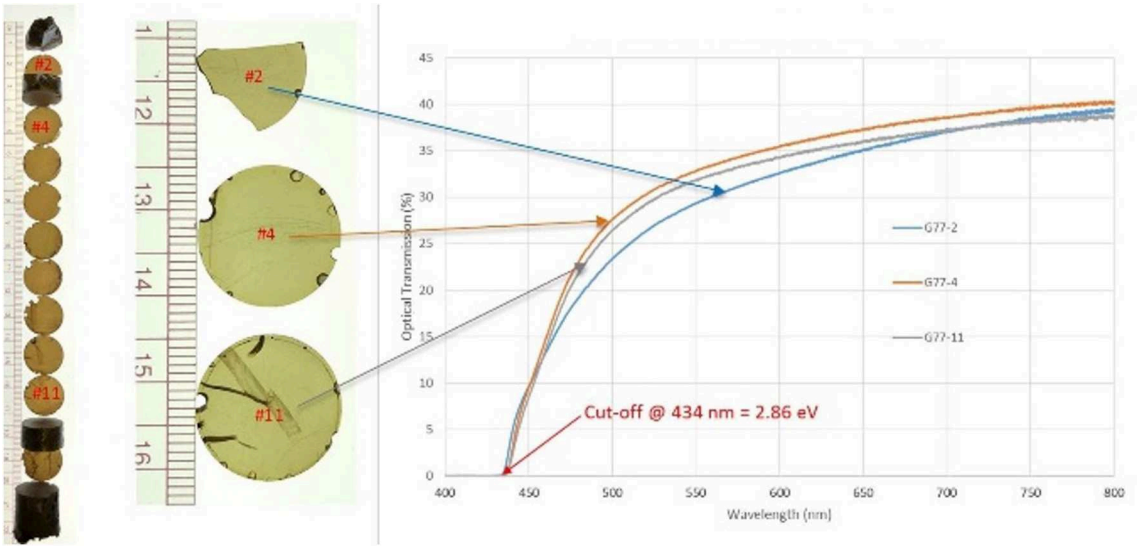

FIGURE 6 | Optical transmission spectra for 0.7 mm thick LiInSe$_2$ crystals sliced from ingot G77. The estimated bandgap is at 434 nm, equivalent to 2.86 eV.

RESULTS

Optical Transmission and Spectroscopy Results

The results of the optical transmission measurements for three samples of ingot G77 are presented in **Figure 6**. The absorption edge was observed at about 434 nm, which corresponds to an energy bandgap of 2.86 eV for LiInSe$_2$ crystals.

Resistivity Results

The current-voltage (IV) characteristic curve obtained from one of the planar devices in **Table 2** (^{6}LiInSe$_2$-G77-6 fabricated from G77 ingot) is presented in **Figure 7**. Note that, this is one of the representatives of the 38 fabricated devices listed in **Table 2**, and one of the 17 devices fabricated with Fe contacts on both sides of the device. As shown, the resistivity of the ^{6}LiInSe$_2$-G77-6 sample was determined to be 3.0×10^{11} Ω cm. Note that the IV curve shows a very linear ohmic behavior. It is known that formation of ohmic contact for a metal-semiconductor interface depends on, the work function WF of metal (Fe in this case being 4.5 eV) and the bandgap of semiconductor (2.86 eV for LiInSe$_2$), the electron affinity of semiconductor and the position of Fermi level within the bandgap (p-type of n-type semiconductor). This ohmic behavior was also observed for other metals applied to LiInSe$_2$ material. Those metals are Au (WF = 5.3 eV), Pt (WF = 5.5 eV) and Cr (WF = 4.5), all forming ohmic contacts on LiInSe$_2$ materials, based on the RMD database summarized in **Table 2**.

Neutron and Gamma-Ray Counting Results

Figure 8 shows spectra for background, ^{241}AmBe neutron source and ^{60}Co gamma-ray source with ^{6}LiInSe$_2$-G77-6 detector. The spectra were taken in 1 h increments with the detector under continuous bias for 21 h to examine the stability over time.

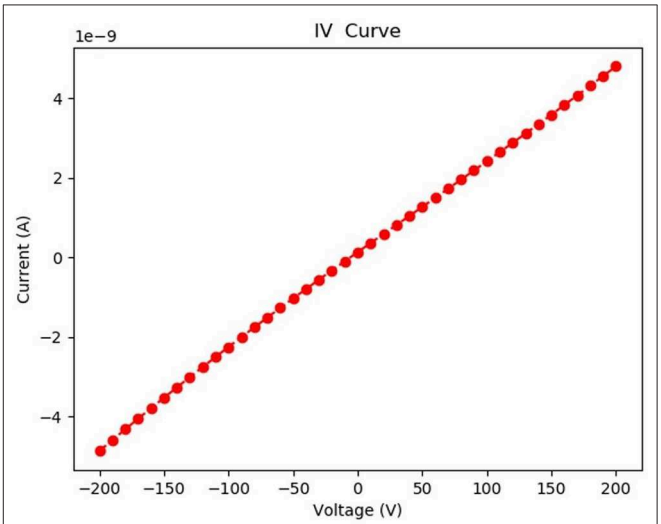

FIGURE 7 | Current-voltage (IV) characteristic curve for ^{6}LiInSe$_2$-G77-6 sample. The resistivity of the sample is evaluated to be 3.0×10^{11} Ω cm, for the sample with 0.7 mm thickness and 8 mm Fe contact diameter.

DISCUSSION

Gamma Rejection Ratio (GRR) is defined as the difference of the gamma-ray (γ) counts and background (BG) above the cut off energy line, over the total counts of gamma rays. Thus, GRR can be written as:

$$\mathrm{GRR} = \frac{\gamma_{>\text{cut off}} - \mathrm{BG}_{>\text{cut off}}}{\gamma_{\text{total}}} \tag{3}$$

The cut off energy line was chosen to be around channel 150, close to the endpoint of ^{60}Co gamma ray energy

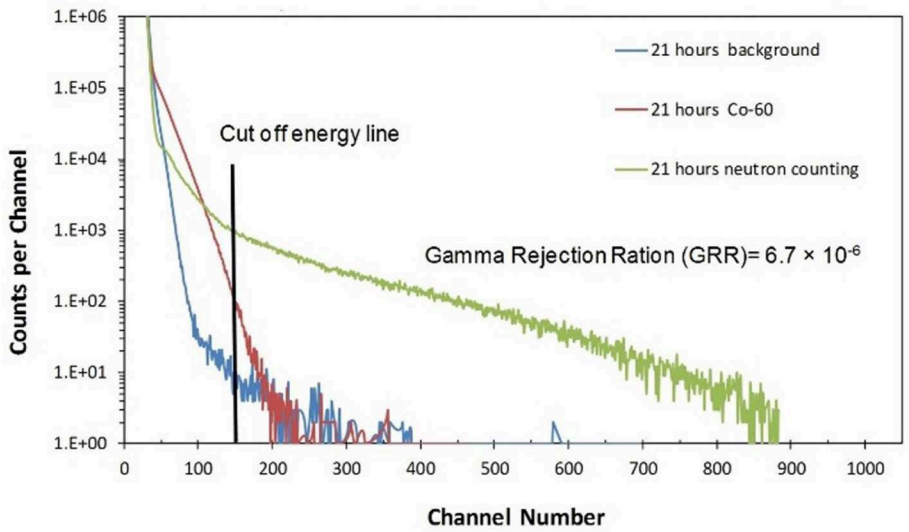

FIGURE 8 | Neutron, gamma-ray, and background spectra of ^{241}AmBe and ^{60}Co obtained over a 21-h period under continuous bias using ^{6}LiInSe$_2$-G77-6 sample with Fe contacts. The cut off energy line was chosen to be around channel 150, close to endpoint of ^{60}Co gamma ray energy line. The GRR was estimated to be around 1.94×10^{-6} for ^{6}LiInSe$_2$-G77-6.

line. The line is shown for the combined spectra for the ^{241}AmBe/^{60}Co neutrons and gamma-rays, and the background for 21 h, as shown in **Figure 8**. By integrating the counts and using the equation above, the GRR was estimated to be around 6.7×10^{-6} for ^{6}LiInSe$_2$-G77-6 sample. The GRR is an important ratio for thermal neutron devices since it indicates the device capability in rejecting the gamma rays, while still detecting the thermal neutrons above the cut off energy line.

CONCLUSION

LiInSe$_2$ semiconductor devices were successfully fabricated and tested for thermal neutron detection purposes. The devices showed response to neutrons emitted from a thermalized ^{241}AmBe source, with decent Gamma Rejection Ratio (GRR) of 6.7×10^{-6}. A compact solid state neutron detection system based on LiInSe$_2$ would be a major breakthrough over conventional thermal neutron detectors, such as ^{3}He tubes that are currently in short supply. This is the long term goal for this study at RMD Inc. Other goals for this research are improving the crystal quality and scaling up the device size. It should be noted that in recent years, other groups have conducted research on Li-based semiconductor devices for thermal neutron detection applications [8–11].

DATA AVAILABILITY STATEMENT

The datasets analyzed in this article are not publicly available. Requests to access the datasets should be directed to Dr. Kanai Shah (kshah@rmdinc.com), since they may contain proprietary information.

AUTHOR CONTRIBUTIONS

All authors listed have made a substantial, direct and intellectual contribution to the work, and approved it for publication.

ACKNOWLEDGMENTS

This work has been supported by the US Department of Homeland Security, Countering Weapons of Mass Destruction Office, under competitively awarded contracts HSHQDC-11-C-00061 and HSHQDC-16-C-00001. This support does not constitute an express or implied endorsement on the part of the Government.

REFERENCES

1. McGregor DS, Unruh TC, McNeil WJ. Thermal neutron detection with pyrolytic boron nitride. *Nucl Instrum Meth A*. (2008) **591**:530. doi: 10.1016/j.nima.2008.03.002
2. Guo L, Xu Y, Zheng H, Xue W, Dong J, Zhang B, et al. Stoichiometric effects on the photoelectric properties of LiInSe$_2$ crystals for neutron detection. *Cryst Growth Des.* (2018) **18**:2864. doi: 10.1021/acs.cgd.7b01705
3. *NIST Center for Neutron Research*. Available online at: http://www.ncnr.nist.gov/resources/n-lengths (accessed May 26, 2011).
4. Kargar, Tower J, Hong H, Cirignano L, Higgins W, Kanai Shah. Lithium and boron based semiconductors for thermal neutron counting. *Proc SPIE.* (2011) **8142**:81421P. doi: 10.1117/12.899363
5. Isaenko L, Yelisseyev A, Lobanov S, Petrov V, Rotermund F, Slekys G, et al. LiInSe2: A biaxial ternary chalcogenide crystal for

nonlinear optical applications in the midinfrared. *Appl Phys.* (2002) **91**:9475. doi: 10.1063/1.1478139
6. Kamijoh T, Kuriyama KJ. Single crystal growth and characterization of $LiInSe_2$. *Cryst Growth.* (1981) **51**:6. doi: 10.1016/0022-0248(81)90003-8
7. Chica DG, He Y, McCall KM, Chung DY, Pak RO, Trimarchi G, et al. Direct thermal neutron detection by the 2D semiconductor $^6LiInP_2Se_6$. *Nature.* (2020) **577**:346. doi: 10.1038/s41586-019-1886-8
8. Tupitsyn E, Bhattacharya P, Rowe E, Matei L, Groza M. Single crystal of LiInSe2 semiconductor for neutron detector. *Appl Phys Lett.* (2012) **101**:202101. doi: 10.1063/1.4762002
9. Stowe AC, Woodward J, Tupitsyn E, Rowe E, Wiggins B, Matei L, et al. Lithium-containing semiconductor crystals for radiation detection. *J Cryst Growth.* (2013) **379**:111. doi: 10.1557/opl.2013.1145
10. Stowe AC, Cochran J, Bhattacharya P, Tupitsyn E, Wiggins B, Groza M, et al. Lithium-containing semiconductor crystals for radiation detection. *Proc MRS.* (2013) 1576. doi: 10.1557/opl.2013.1145
11. Stowe AC, Morrell J, Bhattacharya P, Tupitsyn E, Burger A. Synthesis of a potential semiconductor neutron detector crystal LiGa(Se/Te)2: materials purity and compatibility effects. *Proc SPIE.* (2011) **8142**:81421H−1. doi: 10.1117/12.894968

Conflict of Interest: The authors of this article were employed by company Radiation Devices Inc. (RMD).

The authors declare that the research was conducted in the absence of any commercial or financial relationships that could be construed as a potential conflict of interest.